Earth and Planetary Science Letters 495 (2018) 101–111

Contents lists available at ScienceDirect

Earth and Planetary Science Letters

www.elsevier.com/locate/epsl

Identification of molybdenite in diamond-hosted sulphide inclusions: Implications for Re–Os radiometric dating

Lotta I. Kemppinen [a,*], Simon C. Kohn [a], Ian J. Parkinson [a], Galina P. Bulanova [a], Daniel Howell [a,b], Christopher B. Smith [a]

[a] School of Earth Sciences, University of Bristol, Wills Memorial Building, Queen's Road, Bristol BS8 1RJ, United Kingdom
[b] Vrije Universiteit, De Boelelaan 1085, 1081 HV Amsterdam, the Netherlands

ARTICLE INFO

Article history:
Received 26 June 2017
Received in revised form 15 March 2018
Accepted 18 April 2018
Available online xxxx
Editor: M. Bickle

Keywords:
sulphide inclusions
diamonds
Re–Os dating
molybdenite
Raman spectroscopy

ABSTRACT

Sulphide inclusions are common features of natural diamonds. They can provide an insight into the nature of diamond-forming reactions and are especially important for Re–Os dating of diamond formation. A discrete molybdenite (MoS_2) phase has been identified for the first time by Raman spectroscopy in 73 out of 80 syngenetic sulphide inclusions in 7 eclogitic diamonds from the Mir kimberlite (Yakutia, Russia). The sulphide inclusions were chemically and texturally characterised by electron probe microanalyses (EPMA), focused ion-beam scanning electron microscopy (FIB-SEM) and synchrotron-based X-ray tomographic microscopy (SXRTM). Our observations suggest the molybdenite has unmixed from an original sulphide melt or monosulphide solid solution. It occurs as sub-micron sized grains, commonly in association with the chalcopyrite rims of the inclusions and sometimes, within surrounding decompression cracks. Molybdenite has also been identified by Raman spectroscopy in at least 50% of sulphide inclusions in preliminary studies of eclogitic diamonds from Argyle (NW Australia), Orapa, Letlhakane, Damtshaa (Botswana) and Dachine (French Guiana), and peridotitic diamond-hosted inclusions from Udachnaya (Yakutia, Russia) and Murowa (Zimbabwe). We have modelled the effects that different amounts of Re loss – through its segregation into an unrecovered molybdenite phase – could have on the radiometric ages of diamonds dated using the Re–Os system. In general Re loss through this process will lead to isochron ages older than the true age, and variable degrees of Re loss will lead to increased scatter around the apparent isochron. For model age calculations, the effects would depend on the $^{187}Re/^{188}Os$ ratio of the inclusions (if their compositions evolved above or below that of the chondritic mantle evolution curve) but Re loss could generate unrealistically old or future ages, particularly in eclogitic inclusions.

1. Introduction

Diamond-hosted sulphide inclusions can offer an insight into the processes responsible for diamond formation. Their compositions record mantle melting processes, subduction input and the cycling of volatiles through Earth's interior (e.g. Stachel and Harris, 2008; Walter et al., 2011). Diamond is an ideal container material and can shield mineral inclusions from subsequent alteration and recrystallization events. Therefore syngenetic inclusions, which grew at the same time as the host diamond, can yield valuable information on the geochemical state of their mantle source region.

Diamonds commonly form by different redox reactions (e.g. Haggerty, 1986; Stachel and Harris, 2009) or isobaric cooling of hydrous fluids containing both CH_4 and CO_2 (Stachel and Luth, 2015). Several workers have proposed that sulphides act as reducing agents interacting with oxidised components to promote diamond growth (Bulanova et al., 1998; Palyanov et al., 2007) and, depending on their metal-sulphur ratios, sulphide melts can store significant amounts of carbon at depth (Zhang et al., 2015). Although sulphides are often the most common phase in inclusion-bearing diamonds (e.g. Taylor and Liu, 2009), their overabundance relative to the expected abundance of mantle sulphide remains enigmatic. Diamond-hosted sulphide inclusions are also particularly important because they can be used to date diamond-forming events using the Re–Os chronometer (Pearson et al., 1998; Harvey et al., 2016).

Sulphides typically exist as Fe–Ni–Cu sulphide melts in the deeper parts of continental lithospheric mantle, where most diamonds form (Zhang and Hirschmann, 2016). Upon sub-solidus cooling inside diamond, a Fe-rich monosulphide solid solution

* Corresponding author.
E-mail address: lk15127@bristol.ac.uk (L.I. Kemppinen).

https://doi.org/10.1016/j.epsl.2018.04.037

(MSS) can crystallise from such melts at around ~1200 °C, leaving a residual Cu- and/or Ni-enriched sulphide liquid. At ~1000 °C the MSS field can accommodate more Cu and Ni-rich compositions, and an intermediate solid solution (ISS) can progressively form below ~950 °C (Barton, 1973; Ebel and Naldrett, 1997; Harvey et al., 2016). Depending on their initial composition and pressure-temperature-time history, originally homogeneous sulphide inclusions within the diamonds will unmix into assemblages of pyrrhotite ± pentlandite ± chalcopyrite (Taylor and Liu, 2009; Harvey et al., 2016). During cooling and exhumation, many inclusions develop characteristic rosette-shaped or disc-shaped decompression fractures (Harris, 1972) because of the different equations of state of diamond and sulphide. These fractures may be lined with sulphides (Richardson et al., 2004; Wiggers de Vries et al., 2013a; Harvey et al., 2016) extending outwards from the main sulphide body.

Lithospheric diamonds usually belong to two parageneses: the eclogite (E-type) or peridotite (P-type) suite. These parageneses are distinguished by the silicate or oxide inclusions they contain, indicating whether their main growth substrate was an eclogite or peridotite (Harris, 1968; Shirey et al., 2013). Sulphides in P-type are richer in Ni (> ~12 wt.%; Bulanova et al., 1999) compared to those included within E-type diamonds (Harvey et al., 2016). Eclogitic diamonds frequently contain a component derived from subducted oceanic crust (Schulze et al., 2013).

The majority of samples studied here are eclogitic diamonds from the Mir kimberlite pipe (Yakutia, Russia). They have complex crystallisation histories interpreted in terms of growth under different conditions in a reducing upper mantle environment beneath the Siberian craton (Bulanova et al., 1998). Diamond growth is thought to have occurred in the presence of a fluid which was accompanied by immiscible Fe–Ni–Cu sulphide melts, and their variable inclusion compositions are thought to reflect their source region's changing chemistry (Bulanova et al., 1996, 1998, 2014; Wiggers de Vries et al., 2013a).

The Re–Os geochronology of inclusions in peridotitic diamonds and eclogite xenoliths from the Udachnaya kimberlite gives an Archean age for the Siberian lithosphere (Pearson et al., 1995; Richardson and Harris, 1997). The Mir diamonds are reported to have formed in the Proterozoic in two separate events at ~2.1 and between 0.9–1.1 Ga (Wiggers de Vries et al., 2013a). Rudnick et al. (1993) had also inferred a 1 Ga difference in ages for the core and rim-located sulphides in one Udachnaya peridotitic diamond. Overall, it has been demonstrated that some Yakutian diamonds were formed episodically at <200 Ma intervals through multiple interactions with different evolving metasomatic fluids (Taylor et al., 1998; Wiggers de Vries et al., 2013a, 2013b; Bulanova et al., 2014).

The complex exsolution observed in sulphide inclusions in diamonds has the potential to cause problems with Re–Os age determinations if the whole inclusion is not extracted and dissolved. Chalcopyrite-rich rims have been observed previously (e.g. Bulanova et al., 1996; Anand et al., 2004) and even low abundances of other phases, especially if they are enriched in Re or Os, could lead to significant heterogeneity in platinum group element distribution within the inclusion. Similar issues have been discussed in the literature concerning the validity of using Laser Ablation ICPMS to obtain Re–Os data for sulphides in mantle xenoliths. As well as technical issues surrounding Re corrections (Pearson and Wittig, 2008) several authors have pointed out the importance of sampling the whole inclusion (e.g. Harvey et al., 2016), which is impossible if the inclusion is exposed by polishing. Therefore, laser ablation analyses of sulphides should be avoided for radiometric dating of sulphide inclusions.

In this study we have performed detailed high-resolution Raman spectroscopic mapping of sulphide inclusions and discovered that molybdenite is a relatively widespread, if low in abundance, exsolved phase in many sulphide inclusions in diamonds. The implications of molybdenite unmixing and segregation for Re–Os dating are explored.

2. Material and methods

2.1. Samples

Seven previously studied macrodiamonds from the Mir kimberlite pipe were used in this study (Fig. S1). The characteristics of the samples are described in table S1; the diamonds are colourless, ranging in size from 3 to 6 mm, and define shapes from well-defined to distorted octahedra. Most diamonds display step-layered octahedral faces and minor dissolution features at their edges. Cathodoluminescence (CL) imagery has shown the complex growth history and occasional features of internal resorption of some of the diamonds (Bulanova et al., 1999, 2014; Wiggers de Vries et al., 2013a) (Fig. S2). All diamonds are eclogitic based on the presence of inclusions of eclogitic affinity and their carbon isotopic composition ($\delta^{13}C$) (Table S1). The Mir samples were previously selected, cut and polished for sulphide inclusion study at the Diamond and Precious Metal Institute (Siberian Branch RAS, Russia) but still contain abundant unexposed sulphide and some silicate inclusions (including omphacite, pyrope–almandine garnet and coesite, consistent with the findings of Bulanova et al., 1999). The sulphide inclusions have varying shapes, sizes and fractures associated with them. Some of them exhibit typical rosette-shaped fracture systems around the central sulphide inclusion and others have more discrete and relatively straight cracks surrounding them. All Mir sulphide inclusions examined have a euhedral to subeuhedral body (in a negative diamond crystal shape), and range in size from 2 to 100 µm.

In addition, a few sulphide inclusions in one diamond from Udachnaya (Yakutia), three from Murowa (Zimbabwe), two from Argyle (Australia), two from Dachine (French Guiana), two from Orapa, three from Letlhakane, two from Damtshaa, five from Jwaneng (Botswana) three from Collier-4 and four from Juina-5 (Brazil) were studied, and the presence or absence of molybdenite in these samples will also be reported here.

2.2. Sample preparation

The Mir diamonds were sawn and polished on dodecahedron planes into 1–3 mm thickness plates at the Institute of Geology of Diamond and Precious Metals (Yakutsk, Russia). All the studied inclusions were below the polished surface of the diamond (i.e. were completely encapsulated) before and during Raman measurements. Based on CL imaging and optical microscopy, there appear to be no cracks or healed cracks leading from the inclusions to the diamond surface. All mechanical polishing procedures for exposing inclusions to the surface were completed using an industrial diamond wheel. Molybdenum disulphide was not used at any stage in the preparation of the studied diamonds.

2.3. Analytical methods

2.3.1. Raman spectroscopy

A Thermo Scientific DXRxi Raman imaging microscope was used with blue (455 nm) and green (532 nm) lasers. Laser power of 10 mW was used throughout, with 50 µm or 25 µm confocal pinholes. Long working distance objectives were used throughout (10× and 50×). Exposure times ranged up to 8 s with a maximum of 1000 scans. The blue laser provided better results because of the smaller excitation volume and less interference from diamond luminescence. The spectra were processed with the Raman OMNICxi

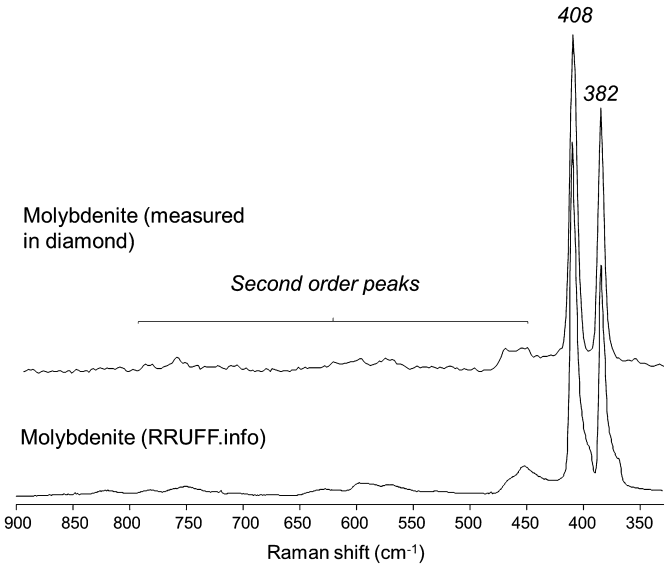

Fig. 1. Comparison of the depolarised 532 nm laser Raman spectra of molybdenite (382, 408 cm^{-1}) measured with a blue 455 nm laser in sulphide inclusions in Mir eclogitic diamonds and a spectrum available on The University of Arizona's online RRUFF mineral spectra database (Lafuente et al., 2015).

software. A diamond signal at 1332 cm^{-1} was present in virtually every measurement.

2.3.2. Electron probe microanalysis (EPMA)

For one sample, an inclusion was exposed by polishing. Wavelength-dispersive spectroscopy (WDS) was undertaken at 30 kV using a Cameca SX100 microprobe with a slightly defocused (~3 µm size) beam to increase the analytical volume.

2.3.3. Focused ion beam SEM (FIB-SEM)

The FIB procedure was undertaken at the Interface Analysis Centre (School of Physics, University of Bristol) using a FEI Helios NanoLab 600 with three-axis micromanipulator, Oxford Inst X-Max50 energy dispersive system (EDS) with 7 nm resolution, platinum deposition and force measurement. During the FIB operation, a maximum beam current of 20 nA and a beam energy of 30 kV were used. EDS measurements were made at 20 and 30 kV. EDS element maps were acquired at 30 kV.

2.3.4. Synchrotron-radiation X-ray tomographic microscopy (SRXTM)

Three of the Mir diamonds were analysed at the TOMCAT beamline at the Swiss Light Source, Paul Scherrer Institut, Villigen, Switzerland. Absorption-Contrast Imaging (ACI) computed microtomography was performed using a 1 µm wide monochromatic beam in conjunction with a 20× objective, producing a voxel (3D pixel) of 0.325 µm, and a 40× objective, producing a voxel size of 0.163 µm.

3. Results

3.1. Raman spectroscopy

Molybdenite has a clear diagnostic Raman spectrum (Mernagh and Trudu, 1993) which has been observed in 73 out of 80 Mir sulphide inclusions (Fig. 1). Molybdenite has two first-order peaks at 408 and 392 cm^{-1}, as well as small second order peaks at ~450, 596 and 757 cm^{-1} (Chen and Wang, 1974). Pyrrhotite (po), which is presumed to be the most abundant sulphide mineral is only weakly Raman active due to its crystal structure and was usually unobservable. The characteristics of some inclusions in Mir diamonds from which a molybdenite Raman signal was obtained are listed in Table S2. Many of the diamonds contain several sulphide inclusions that are distributed from the core to rim zones. There is no discernible correlation between the position of the inclusion within the diamond and the presence or absence of molybdenite. Maps of the 408 cm^{-1} peak intensity for various inclusions with spatial resolutions of 0.6–0.8 µm were produced, with examples shown in Fig. 2. The maps show the distribution of molybdenite (red areas show where its Raman signal is most intense) but cannot be used to quantitatively assess the volume fraction of molybdenite in the inclusion because of potential scattering of the laser light, absorption of the laser by opaque phases and focusing limitations. Nonetheless, the data show unambiguously that molybdenite is widespread in the inclusions. It appears to form small (typically around 1 µm) and unevenly distributed grains, often seen near the edges of the sulphide inclusions. Molybdenite is commonly manifested as an irregular film near the inclusion walls (e.g. Fig. 2A).

In 61 out of 80 inclusions, molybdenite is found closely associated with chalcopyrite, possibly in an intergrowth relationship (e.g. Fig. 2B). Chalcopyrite is also commonly seen inside the decompression cracks surrounding an inclusion, where the material present can exhibit patchy or weave-like textures. Diamond 1702 hosts a cluster of molybdenite-bearing sulphide inclusions in its core. A Raman signal for pyrrhotite (Fig. S3) was obtained in the fractures surrounding most of these, where chalcopyrite and molybdenite are also present. Fig. 2C shows an inclusion in the rim zone of diamond 1702, which hosts molybdenite within its body while the cracks contain chalcopyrite.

An inclusion located in the intermediate zone of diamond 1703 (inclusion 1) contains omphacite adjacent to a non-Raman-active sulphide, but no molybdenite was detected. The inclusion is partially exposed, having lost some of its rim portions. Molybdenite is, however, found inside the sulphide inclusions that occur in the outer intermediate zone (zone of resorption and regrowth) of this diamond (Fig. S2).

Fig. 3A shows sulphide inclusion 1704-2 oriented to the Raman optical microscope light in such a way that a dark phase with a mottled appearance can be seen on the surface of a hexagonal inclusion body (Fig. 3B). Although the typically rhombohedral crystal shape of molybdenite cannot be discerned, Raman peak height maps show its presence is restricted to this surface (Fig. 3C). Molybdenite (that seems to be in the form of plates with a maximum diameter of 3 µm) is also found within the rosette fractures surrounding this inclusion: the distribution of molybdenite in the inclusion's cracks, as shown by Raman peak height maps (Fig. 3E), coincides with the pale-coloured points visible in transmitted light (Fig. 3D).

Fig. 4A shows sulphide inclusion 1584r-3 which exhibits a negative diamond shaped-body connected to relatively straight disc-shaped decompression cracks. A Raman peak height map in Fig. 4B indicates that molybdenite is present. As the penetration depth of the blue laser light into the opaque sulphide inclusion is low, the observation of molybdenite peaks indicates that molybdenite is located at the surface of the inclusion. Molybdenite could also be present inside the inclusion body, but would be unobservable. In this example, no material was found inside the inclusion's fractures. In addition to molybdenite, the inclusion also contains chalcopyrite (Table S2). The diamond was polished in an attempt to expose the molybdenite for further analyses. Subsequent Raman peak height maps showed that the molybdenite was still present in some of the unexposed portions of the inclusion, very close to the edge of the exposed surface. However, no molybdenite was observed at the polished surface, possibly because it is so soft that it is removed as soon as it is exposed.

In summary, we have studied 80 sulphide inclusions in 7 diamonds from the Mir pipe using Raman, and of these, 73 inclusions clearly contained molybdenite. This is a minimum number, because

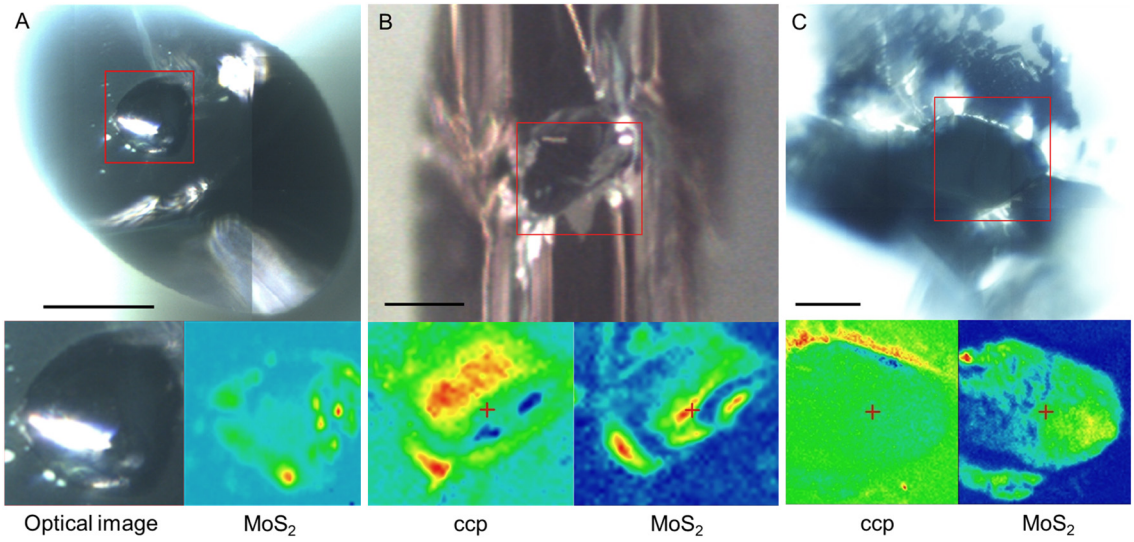

Fig. 2. Optical images and Raman maps of molybdenite-bearing sulphide inclusions. The Raman maps are based on the baseline-corrected peak heights at 408 cm^{-1} peak for molybdenite and 293 cm^{-1} for chalcopyrite. The colour scaling was chosen to best represent the distribution of each phase; otherwise the colour scales are arbitrary and not comparable between images. Red indicates where the signal for the mapped phase is most intense. Yellow and green colours show areas where the signal is present, but weaker and/or barely detected). A) In diamond 1584-i, the body of an inclusion contains molybdenite (MoS_2) forming irregular disseminations at its edge. Scale = 50 µm. B) In inclusion 1704-2, chalcopyrite (ccp) and molybdenite appear to be intergrown. Scale = 30 µm. C) An inclusion in diamond 1702 is surrounded by rosette fractures lined with patchy intergrowths of dark material presumed to be sulphide and/or graphite. Raman peak height maps show the occurrence of molybdenite at the edge of the inclusion body while chalcopyrite is found in the decompression fractures. Scale = 50 µm. (For interpretation of the colours in the figure(s), the reader is referred to the web version of this article.)

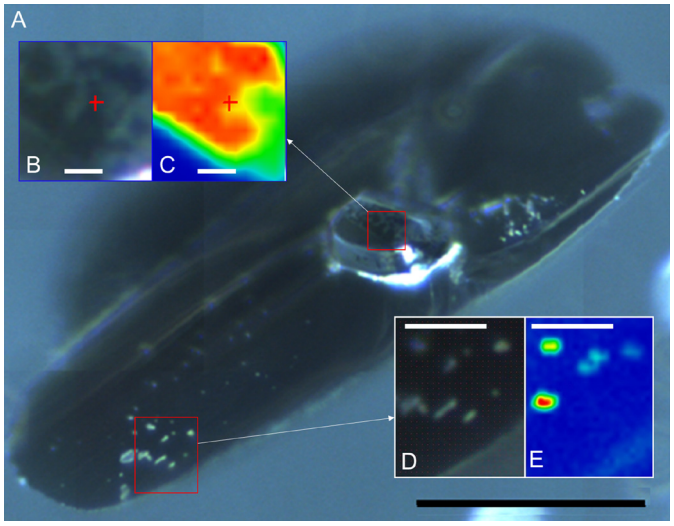

Fig. 3. A) Optical microscope image of inclusion 1704-2. The hexagonal body of the inclusion exhibits dark patches on its surface, a higher magnification view of which (B) and corresponding Raman map of molybdenite distribution (C) are provided; molybdenite is distributed in the area where the dark mottled phase occurs. The inclusion is surrounded by planar decompression fractures, speckled with pale yellow grains (magnified in D). The corresponding Raman map in E shows molybdenite forming in points within the decompression fractures (Scale bars: A = 50 µm; B, C = 5 µm; D, E = 10 µm). The significance of the colours in the Raman maps is explained in the caption to Fig. 2.

it is possible that in other inclusions molybdenite was present, but undetected because it was obscured by other opaque sulphides. So, at least 90% of studied Mir sulphide inclusions contain molybdenite, hence it cannot be considered to be a mineralogical oddity; this observation has major implications for the analytical techniques used in the study of trace element abundances and Re–Os geochronology of sulphide inclusions in diamond. Additional techniques were therefore applied in order to obtain a better understanding of the molybdenite distribution.

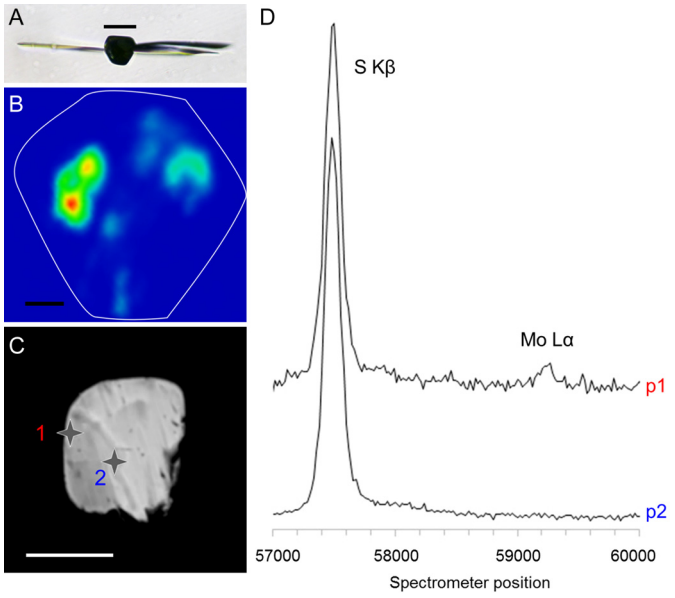

Fig. 4. A) Optical plane-polarised image of unexposed inclusion 1584-r-3 shows a hexagonal inclusion body connected to disc-shaped decompression fractures. B) The Raman map shows the location of molybdenite inside the *unexposed* inclusion (the outline of which is drawn in white). The molybdenite is at the top surface of the inclusion in this projection. All the Raman signal originates from the surface of the inclusion as the laser light does not penetrate a significant depth into the opaque sulphide inclusion. C) Back-scattered electron (BSE) image of *exposed* inclusion 1584-r-3 showing the location of WDS point measurements 1 and 2 (grey crosses). Scales are 30, 5 and 10 µm in A, B and C respectively. D) WDS spectrum from point 1 (red) shows Molybdenum (Mo) enrichment relative to point 2 (blue). The y axis of the spectrum at point 2 has been scaled down by ~3.5, to make the sulphur K-beta (S Kβ) peaks in both spectra the same height. Less sulphur was measured at point 1 because of its proximity to the edge of the inclusion and presence of diamond.

3.2. EPMA and FIB-SEM

Exposed inclusion 1584-r-3 was studied by electron probe microanalysis (EPMA), but no features attributed to molybdenite

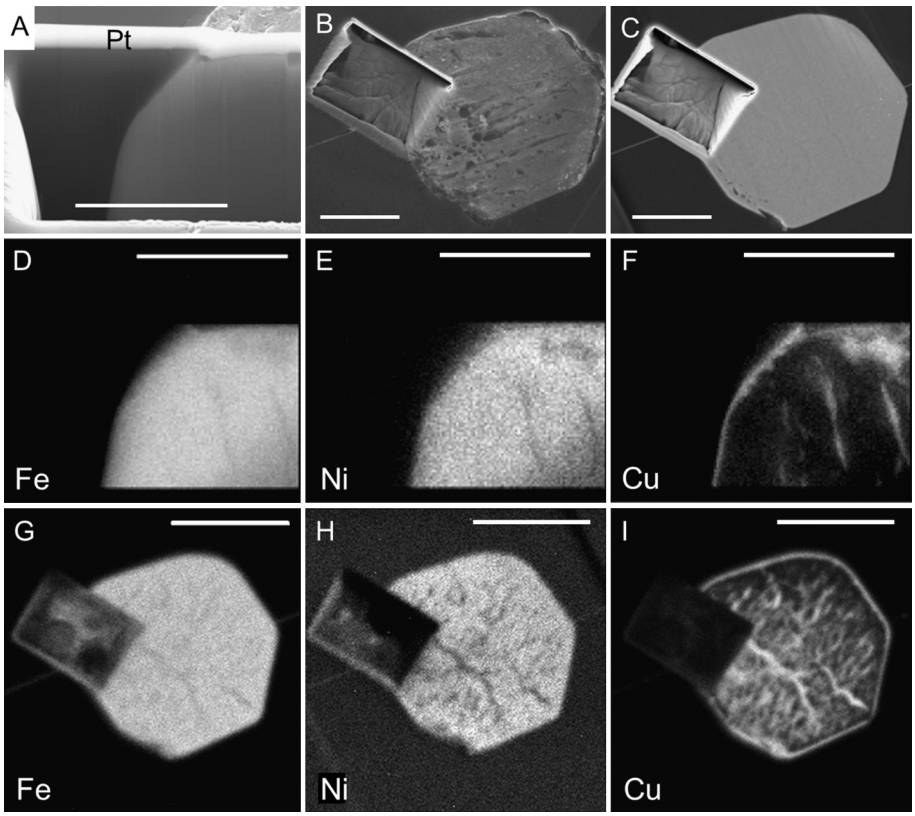

Fig. 5. A) Back-scattered electron image of a Focused-Ion Beam (FIB) cross-section of exposed inclusion 1584-r-3 (Pt refers to the line of platinum deposition). Back-scattered electron images are also provided to show the surface of inclusion before (B) and after (C) FIB cleaning. The rectangular feature in B and C is the FIB trench, the wall of which is shown in A. EDS X-ray element maps (at 30 kV) show the distribution of Fe, Ni and Cu in sulphide inclusion 1584-r-3, parallel to the FIB-trench wall (D–F) and parallel to the polished exposed surface (G–I). X-ray maps show a Cu-rich rim and lamellae in a seemingly homogeneous Fe–Ni sulphide matrix. The scales = 8 (A, D, E and F), 15 (B and C) and 20 μm (G, H and I).

were observed by back-scattered electron (BSE) (Fig. 4C) or X-ray imaging of the exposed inclusion surface. The sulphur Kα peak overlaps with that of molybdenum L-lines so energy dispersive spectroscopy (EDS) cannot be used. Wavelength-dispersive spectra (WDS) were therefore obtained from near the edge of the inclusion wall (point 1) and the centre of the inclusion (point 2) (the locations are shown Fig. 4C). WDS spectra in Fig. 4D show that Mo is concentrated near the edge of the inclusion, although pure MoS_2 could not be identified presumably because the MoS_2 particles are much smaller than the analysed volume (~3 μm).

Fig. 5A shows the ~20 μm wide FIB-SEM section that was produced to study the diamond/sulphide interface of inclusion 1584-r-3. The inclusion was polished by focused-ion beam milling to achieve a cleaner surface (Fig. 5B and 5C). The FIB cross-section was imaged by EDS X-ray mapping (Fig. 5D, 5E and 5F), but no MoS_2 was observed in the Mo element maps at 30 kV, again suggesting that the abundance is very low. It should be noted however, that molybdenite is a particularly soft sulphide, and could have been sputtered away during FIB-polishing. EDS X-ray maps were also acquired parallel to the polished surface (Fig. 5G, 5H and 5I). Maps of both FIB-polished surfaces reveal an iron and nickel-enriched matrix with exsolved Cu-rich lamellae; these very clearly show the exsolution of chalcopyrite in veins and, crucially, at the rim of the inclusion.

3.3. SXRTM (X-ray tomography)

A total of 32 unexposed molybdenite-bearing sulphide inclusions within diamonds 1584-r, 1591 and 1607 were analysed by synchrotron-based X-ray microtomography. Absorption Contrast Imaging (ACI) results presented in Fig. 6 show a complex network of cracks radiating from the body of 29 of these inclusions (e.g. Fig. 6A and 6B). The decompression fractures surrounding the inclusions contain high-density (bright) sulphide. Most of the inclusions also exhibit features resembling exsolution of a lower-density (darker) material within the sulphide body (Fig. 6C). In two cases, the sulphides contain fractures that do not extend into diamond. Most of the sulphide inclusions analysed in diamonds 1591 and 1607 exhibit relatively uniform textures, with discrete lower density exsolution features near the inclusion walls. Although molybdenite could not be positively identified by SXRTM, the data clearly show the complex unmixing and extrusion of sulphide material along cracks.

3.4. Occurrence of molybdenite in different types of diamonds

The common occurrence of molybdenite in Mir diamonds (>90% of inclusions) raises important questions about previous interpretations of sulphide inclusion compositions in diamonds. We have found one previous report of molybdenite in diamond; Davies et al. (2002) discovered molybdenite included in a grossular garnet inclusion from a New South Wales alluvial diamond. To assess whether molybdenite is an ubiquitous phase, or unique to the eclogitic paragenesis, a total of 35 inclusions in 27 samples from 10 other suites, including both eclogitic and peridotitic diamonds, were studied. So far, we have identified molybdenite in 3 out of 3 sulphide inclusions and an inclusion cloud in 1 peridotitic diamond from Udachnaya, 3 out of 3 inclusions in 3 peridotitic diamonds from Murowa (Zimbabwe), 2 out of 2 inclusions in 2 eclogitic diamonds from Dachine (French Guiana), 3 out 7 inclusions in 3 eclogitic diamonds from Argyle (Australia), 2 out of 3 inclusions in 2 diamonds from Orapa (Botswana), 2 out of 2 in-

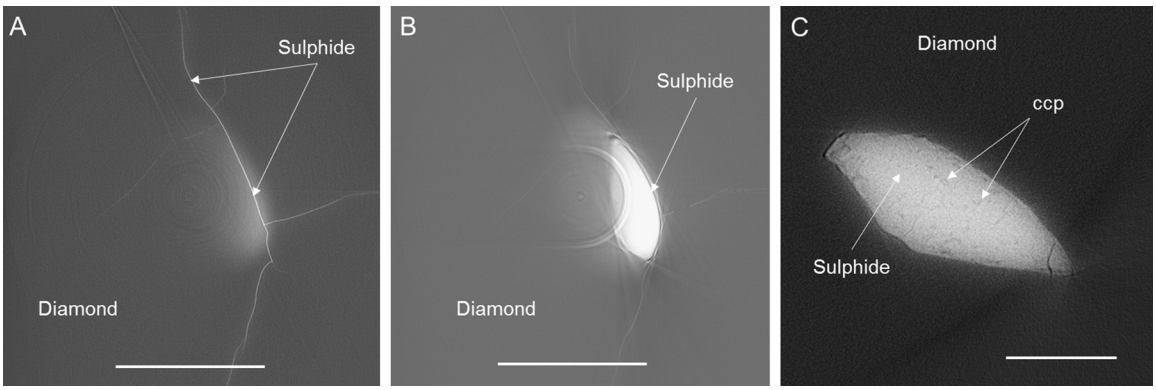

Fig. 6. Synchrotron-based X-ray tomographic microscopy (SXRTM) images through molybdenite-bearing sulphide inclusions in diamond (original pixel size = 0.163 μm). Absorption Contrast Imaging (ACI) detects density differences between different higher-density (bright) sulphide and lower-density (darker) diamond. A) Sulphide infills the rosette fractures radiating from the body of an inclusion in diamond 1591 (the main body of the inclusion is not seen in this slice of the 3-D image). B) A slice taken 10 μm from (A) showing the body of the sulphide inclusion. C) A sulphide inclusion in diamond 1584-i contains meandering lamellae of a darker, lower-density sulphide (chalcopyrite, ccp) within a brighter, higher density matrix (presumed Fe–Ni sulphide). The scales = 20 μm.

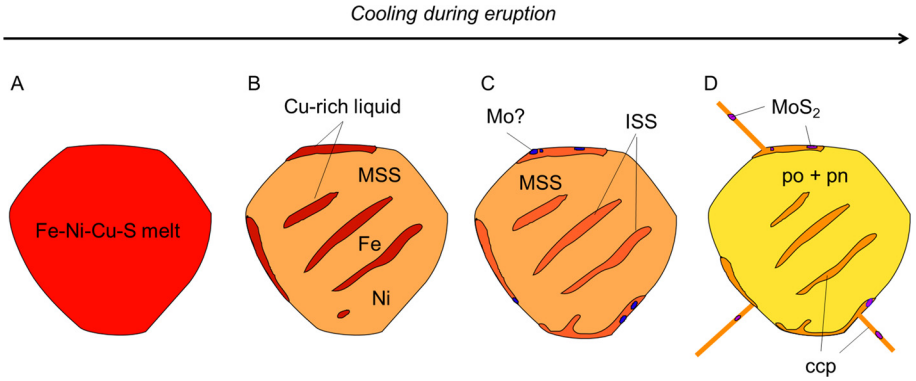

Fig. 7. Simplified model of sulphide exsolution within molybdenite-bearing inclusion 1584-r-3. (A) The inclusion is trapped as melt before (B) exsolving into different phases, including a Cu-enriched liquid and monosulphide solid solution (MSS). Upon further cooling (C) the residual melt crystallises to intermediate solid solution (ISS) and possibly a Mo-bearing phase. On final cooling to room temperature (D) further unmixing produces a pyrrhotite (po) groundmass, closely associated with a discrete Ni-phase (e.g. pentlandite, pn), chalcopyrite (ccp) veinlets and rim and peripheral molybdenite (MoS_2) some of which is extruded along fractures (in D). For simplicity, the represented volumes of Cu-rich liquid, ISS and ccp are almost the same in (B), (C) and (D) respectively, although the small differences in composition between the phases will lead to some changes in relative mineralogical modes. Most of the steps in this scheme (including crystallisation of molybdenite) are thought to occur upon ascent of the diamond during kimberlite eruption.

clusions in 3 diamonds from Letlhakane (Botswana) and 2 out of 3 inclusions in 2 diamonds from Damtshaa (Botswana). However, molybdenite has not yet been seen in any of 7 inclusions in 5 diamonds from Jwaneng (Botswana) or in 7 studied sulphide inclusions from sub-lithospheric diamonds from Collier 4 and Juina-5 (Juina kimberlite field, Brazil). The reasons for the presence or absence of molybdenite is not yet clear. The presence of molybdenite in inclusions from both peridotitic and eclogitic diamonds implies that enrichment of Mo in sulphides to a level that causes molybdenite exsolution is not related to any specific paragenesis. Factors such as different sources of materials for sulphide and silicate inclusions or variations in oxygen fugacity may instead play a role.

4. Discussion

4.1. Unmixing from a sulphide melt

Sulphides mainly exist in molten form at the formation pressures and temperatures of lithospheric diamond formation, although under cooler conditions crystalline monosulphide solid solutions could also occur (Sobolev, 1974; Li and Audétat, 2012; Zhang and Hirschmann, 2016). The composition of mantle sulphide liquids would be significantly different from MSS (particularly in terms of Cu concentration), therefore if a sulphide liquid is trapped in diamond there are two possible scenarios for the period between diamond growth and exhumation depending on the prevailing conditions: (i) the inclusion consists of a sulphide liquid only; (ii) the liquid partially crystallises to MSS and Cu-rich residual liquid. It is likely that further changes in sulphide mineralogy only occur during exhumation of the diamond to the surface by kimberlite transportation, and subsequent cooling. Raman data (Figs. 2 and 3) and X-ray element maps (Fig. 5) of molybdenite-bearing sulphide inclusion 1584-r-3 are consistent with unmixing from an original Fe–Ni–Cu–Mo sulphide melt. In this section we will describe the likely changes occurring if sulphide inclusions are trapped as liquids, although the unmixing pathway would be similar if the trapped sulphide is MSS.

The proposed post-entrapment crystallisation sequence is illustrated in Fig. 7. Following the trapping of sulphide liquid (Fig. 7A) a Fe-rich MSS is the first solid to crystallise from melt at about 1200 °C, leaving a residual Cu-enriched sulphide liquid (Barton, 1973; Ebel and Naldrett, 1997) (Fig. 7B). Upon further cooling below ~950 °C, a Cu-rich intermediate solid solution (ISS) may develop (Ebel and Naldrett, 1997). Either Mo is partitioning into the Cu-rich phase, or a separate Mo-rich phase crystallises around the same time (Moh, 1978). It is not clear which of these processes is dominant, but ultimately the Mo is segregated into molybdenite at the edge of the inclusion. The textures observed in the SXRTM data of molybdenite and chalcopyrite-bearing inclusions (Fig. 6) show that some sulphide inclusions in diamond (e.g. 1584 in Fig. 6C) have a higher proportion of chalcopyrite than others, perhaps re-

flecting a different source or simply trapping as sulphide melt rather than Fe-rich MSS. The details of the exsolution pathway are uncertain, because the phase equilibria of sulphide systems at high pressure are not well known. Moh (1978) showed that the liquid eutectic of the Cu–Mo–S system at 1 bar occurs at 1063 °C and phases in the Fe–Cu–Mo–S sulphide system can begin to crystallise around 1000 °C (Moh, 1978). There is no data on the analogous system including Ni.

Finally, the system of fractures develops around the inclusions. Molybdenite and chalcopyrite are disproportionately sequestered into the cracks because they occur at the edges of the inclusions (Fig. 7D). Perhaps the ductility of molybdenite (Anthony et al., 2003) also plays a role in the injection of molybdenite deep into the narrow fractures.

The range of formation temperatures established for Siberian eclogitic diamonds spans the range of coexistence of sulphide melts and MSS crystals (e.g. Sobolev, 1974) and variable fluid compositions could also influence sulphide solidii. As shown by the CL zonation of many of the Mir diamonds, the different diamond zones may have grown under distinct thermal or chemical conditions, thus in the same Mir diamond population it is possible that some inclusions were captured as Fe-rich MSS and others as sulphide melt. It is tempting to speculate that sulphide trapped as melt may contain more Mo than sulphide trapped as MSS, but more work would be required to confirm this idea.

4.2. The potential effect of molybdenite on Re–Os systematics

There is a distinct possibility that the molybdenite inside fractures in particular, will not be recovered for dissolution and analysis. The recognition that molybdenite is commonly associated with sulphide inclusions in diamonds has important implications for Re–Os dating of the inclusions, because Re will be strongly partitioned into molybdenite relative to the rest of the sulphide inclusion, whereas Os will be retained in the inclusion. When the diamond is 'cracked open' to retrieve the inclusion for Re–Os dating, there is a distinct possibility that the molybdenite inside fractures in particular, will not be recovered for analysis. Any molybdenite would be modally insignificant, and may be invisible under a microscope. Here we will explore the implications of not recovering the molybdenite for Re–Os dating of sulphide inclusions.

The decay of ^{187}Re to ^{187}Os has been used to date inclusions in diamond based on their measured ratios of parent ^{187}Re and daughter ^{187}Os to non-radiogenic ^{188}Os. These compositions can be plotted and a best fit regression can then be derived to determine an isochron age; alternatively model ages (T_{MA} or T_{RD}) can be calculated with reference to chondritic ^{187}Re/^{188}Os and ^{187}Os/^{188}Os ratios (Harvey et al., 2016).

Because Re partitions strongly into molybdenite relative to Os (e.g. Stein et al., 2003), ^{187}Os and ^{188}Os would both remain in the sampled part of the inclusion, but a disproportionate amount of parent Re would potentially be lost from the sampled inclusion. Re-loss could potentially lead to incorrect dates being calculated, because the measured Re contents, contributing to the measured radiogenic Os would be lower than in the parental sulphide, so the ^{187}Os/^{188}Os ratio would be unsupported by the measured ^{187}Re/^{188}Os ratio. However, the details of how dates would be affected depend on many factors:

i) The modal abundance of molybdenite in the inclusions (controlled by the bulk Mo concentration of the inclusion and the solubility of Mo in the non-molybdenite phases).
ii) The proportion of molybdenite missed when extracting the inclusion.
iii) The bulk Re and ^{187}Re/^{188}Os ratio of the inclusion.
iv) The partition-coefficient of Re between molybdenite, chalcopyrite and the residual sulphide inclusion.
v) The timing of molybdenite exsolution (i.e. shortly after trapping of the inclusion, or during diamond exhumation by kimberlite).
vi) The method of age determination (Re/Os isochron age versus Re/Os model age).

4.2.1. Modelling the partitioning of Re into Mo-bearing sulphide

To model the potential distribution of Re between molybdenite and the coexisting sulphides, we have estimated how much molybdenite could form from sulphide melt trapped inside diamond. We consider the scenario of sulphide inclusions trapped as a homogeneous Fe–Ni–Cu–Mo sulphide melt ultimately forming molybdenite upon eruption and unmixing. The reported Mo concentration in sulphide inclusions in diamonds is around 10–700 ppm, (Bulanova et al., 1996; Wiggers de Vries et al., 2013a; Aulbach et al., 2012). If 120 ppm Mo (the mean of the reported values) were exsolved as MoS_2, this would correspond to 0.02 wt.% MoS_2.

Due to the similar geochemical properties of Re^{4+} and Mo^{4+}, molybdenite hosts Re in higher concentrations relative to other sulphides. Published concentrations of Re in molybdenite relative to coexisting iron and copper sulphides (e.g. Mathur et al., 2002; Barra et al., 2003; Zu et al., 2015) were used to approximate the partition coefficients used in our model. The derived Re partition-coefficient for molybdenite relative to chalcopyrite and pyrrhotite is in the range 5000–190000. Fig. 8A shows the percentage of Re that remains in the residual sulphide (po, ccp etc.) as a function of the modal percentage of molybdenite, modelled with partition coefficients between 5000 and 100000. For realistic parameters as much as 95% of the Re could be sequestered in molybdenite (although not all of it need be lost during extraction of the inclusion).

Further calculations have been performed to explore the relative importance of molybdenite and chalcopyrite in hosting Re. Surprisingly the Re partition-coefficient for chalcopyrite/pyrrhotite is rather poorly known. Studies of coexisting chalcopyrite and pyrrhotite in mineral deposits (Barnes et al., 2006; O'Driscoll et al., 2009; Piña et al., 2012, 2016; Wang et al., 2015) suggest that Re has a small preference for pyrrhotite, with partition coefficients $D_{Re}^{po/ccp} = \sim 1.5–56$. This contrasts with literature concerning unmixed sulphide inclusions in diamonds, which always states that Re is enriched in chalcopyrite relative to pyrrhotite. The latter idea originates from the study of Richardson et al. (2001) which measured the Re concentrations in a Cu-rich fragment from the edge of a sulphide inclusion and a Cu-poor part of the same inclusion. It was found that the Re concentration was higher in the Cu-rich part and it was therefore assumed that Re partitions into chalcopyrite. Our calculations using the Richardson et al. (2001) data and assuming that both fragments of inclusion DP9 contained only pyrrhotite and chalcopyrite suggest a value of $D_{Re}^{ccp/po} \approx 2$. Furthermore, the time-resolved laser-ablation data of McDonald et al. (2017) suggest that Re is enriched at the Cu-rich edges of unmixed inclusions. However, the results of our study could suggest that in fact the higher Re concentration in both studies resulted from the incorporation of small amounts of Re-rich molybdenite along with Re-poor chalcopyrite from the edge of the inclusion. Bearing in mind these considerations we have modelled the partitioning of Re between the three main phases with 5% chalcopyrite and values of $D_{Re}^{ccp/po}$ in the range 0.5–5 and $D_{Re}^{mo/MSS} = 5000–100000$ (Fig. 8B and 8C). In these figures we consider the extreme case that all the MoS_2 and ccp is lost from the inclusion during the extraction process and the more realistic scenario that 10% of the ccp and 50% of the MoS_2 are lost during extraction. Obviously less Re is lost in the latter case, but even with conservative assumptions about partition coefficients and the mode of lost MoS_2 and ccp, the Re loss could be very significant (Fig. 8B). The relative importance of MoS_2 and

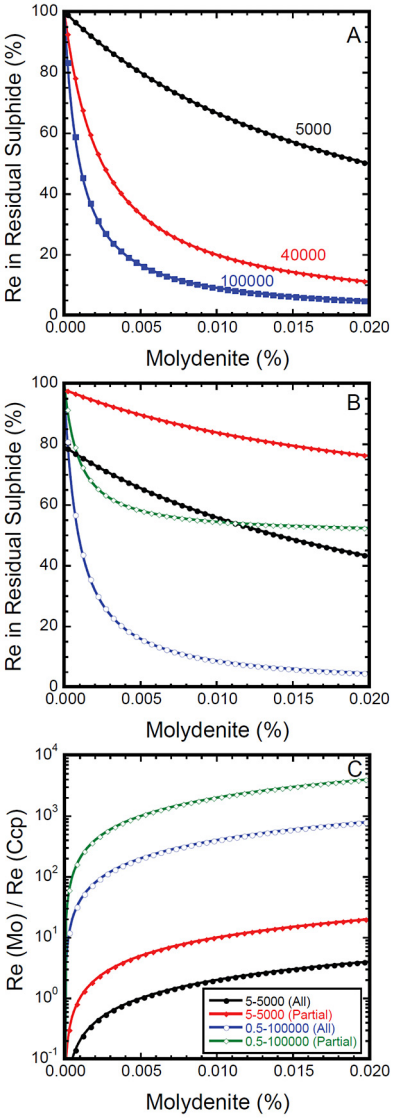

Fig. 8. (A) Model defining the relationship between the amount of molybdenite in a sulphide inclusion and the proportion of Re remaining in residual sulphide (MSS + chalcopyrite + pentlandite etc.) for different partition coefficients, $D_{Re}^{mo/MSS}$ (5000, 40000 and 100000) worked out from literature (see section 4.2.1). (B) and (C) consider partitioning of Re between three coexisting phases, molybdenite, chalcopyrite and pyrrhotite, where the mode of chalcopyrite is set to 5%. (B) shows the percentage of Re in the residual po (i.e. excluding the Re hosted in unrecovered MoS_2 and ccp) and (C) shows the relative importance of MoS_2 and ccp for hosting Re. In (B) and (C) two scenarios are modelled, either all the Re in MoS_2 and ccp is lost from subsequent analysis (labelled "All" in the legend and considered to be an extreme assumption that is unlikely to be true) or 10% of the ccp and 50% of the MoS_2 are lost (labelled "Partial" in the legend and a more realistic possibility). For both cases two extreme combinations of partitioning are used in the model, either a high value of $D_{Re}^{ccp/po}$ (5) and a low value of $D_{Re}^{mo/po}$ (5000) or a low value of $D_{Re}^{ccp/po}$ (0.5) and a high value of $D_{Re}^{mo/po}$ (100000). The legend in (C) also applies to (B).

ccp for Re loss is explored in Fig. 8C. For all the scenarios modelled here, MoS_2 is more important for Re loss than ccp with any MoS_2 mode above 0.005%. For the reasonable values of 0.02% MoS_2 in the inclusion, 10% loss of ccp and 50% loss of MoS_2 with partition coefficients of $D_{Re}^{ccp/po} = 0.5$ and $D_{Re}^{mo/po} = 100000$, MoS_2 is 4000 times more effective than ccp in causing Re loss from the analysed part of the inclusion.

One final complication would pertain if the crystallisation and unmixing occurred faster than the rate of reequilibration. In that case the key process would be the partitioning of Re between MSS and a Cu-enriched liquid. Experimental data and observations on

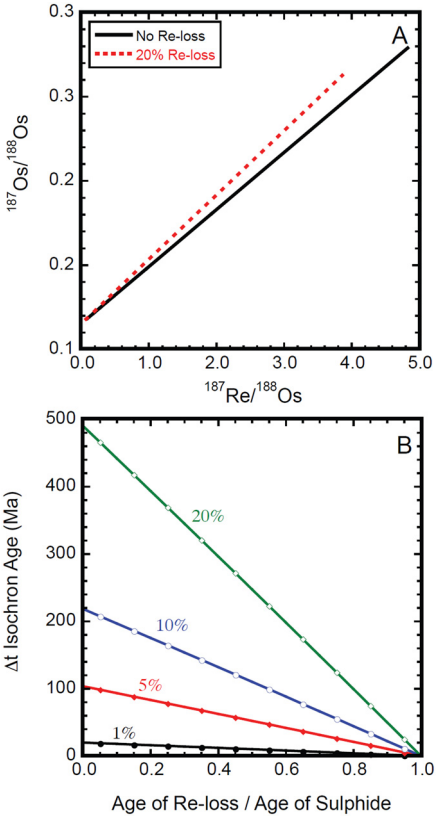

Fig. 9. A) Isochron plot illustrating the effect of Re-loss, which is to increase the slope and therefore calculated age. B) Plot of the difference in isochron age from the true age (Δt) as a function of the timing of the Re-loss relative to the true age of the sulphide. In this calculation the true age of the sulphide was 2000 Ma, but Δt scales linearly with true age (i.e., for the same model parameters, if the true age was 1000 Ma, Δt would be half the value plotted in the figure). The four lines correspond to four different degrees of Re loss, 1, 5, 10 and 20%.

natural samples (Brenan, 2002; Barnes et al., 2008) imply that Re is compatible in MSS ($D_{Re}^{MSS/liquid} \approx 2.5–9$) and this would lead to higher Re in pyrrhotite (crystallised from MSS) than chalcopyrite (crystallised from ISS, which itself would have crystallised from the liquid).

4.2.2. *Modelling the effects of Re-loss on radiometric ages*

Dating of sulphide inclusions can be accomplished by producing an isochron, from co-genetic inclusions. Alternatively ages can also be derived using the model age equation by making assumptions about the initial isotope composition (usually a chondritic mantle). While the isochron method is preferable, much published dating of individual sulphide inclusions in diamonds has by necessity also used the model age method. Our work suggests that the molybdenite is formed at the time that the kimberlite host for the diamond/inclusion is erupted. In most cases this eruption is significantly later than the putative age of the diamond. Therefore, it is worthwhile undertaking some simple calculations to illustrate the effects of Re-loss on isochron and model age determinations.

Any form of open system behaviour will compromise an isochron and detection of this behaviour is assessed by the quality of fit of the isochron (mean square weighted deviate; MSWD). Taking the simplest possible effect of Re-loss, which is that the proportion of Re-loss is equal for each sulphide, will maintain both the quality of fit and value of the intercept of the isochron (see Fig. 9A). However, the isochron will give an age greater than the true age as Re-loss rotates the isochron anti-clockwise (steepens the slope). This increase in isochron age occurs irrespective of whether the points have Re/Os ratios greater or less than chon-

dritic mantle (see discussion below). Fig. 9B illustrates the effect of variable amounts of Re-loss on the isochron age by parameterising the ratio of when the Re-loss occurred relative to the true age of the sulphides. The calculations indicate the isochron age will increase with both increasing Re-loss and increasing time of Re-loss relative to the initial formation age of the sulphide. In nature, it is highly unlikely that each sulphide would lose proportionally the same amount of Re (or the recovery of molybdenite is equally efficient). The effect of variable Re-loss is to reduce the quality of the fit of the isochron and can produce an incorrect initial $^{187}Os/^{188}Os$ ratio. Modelling (not shown here) suggests that as little as 5% relative variability in the Re-loss of sulphides would produce isochrons with MSWDs significantly greater than 2.5. This may explain why many published isochrons for sulphide inclusions from diamonds have MSWDs with values greater than 10.

The effect of Re loss on Re–Os model ages depends on whether the sulphide inclusion evolved with a Re/Os greater or less than the chondritic mantle. If the included sulphides evolve with a Re/Os ratio less than chondritic mantle, the evolution curve has a shallower slope than the mantle evolution curve. If Re loss occurs at some time after the formation of the sulphide it will then evolve along an even shallower slope. The resultant model age (T_{MA}) must always be younger than the true age of the sulphide (see Fig. 10A). By contrast, when a sulphide has a Re/Os ratio greater than chondritic mantle, the sulphide will initially evolve on a steeper curve than the primitive mantle. Loss of Re at some point after formation of the inclusion will produce model ages with a greater age than the true age of the sulphide. However, there is a critical amount of Re loss whereby the model age will exceed that of the age of the Earth. Increasing loss will produce unrealistic ages until the model age line comes into parallelism with the mantle evolution curve and there is no solution. Further Re loss then produces future ages (Fig. 10B).

In a similar manner to the isochron calculation we have calculated the deviation in the model age from the true age as a function of the timing of Re-loss, but also the initial $^{187}Re/^{188}Os$ ratio. Some representative calculations are illustrated in Fig. 10C, with $^{187}Re/^{188}Os$ ratios from 0.3–10. Increasing the Re-loss will increase the disparity in the age as will increasing the time between Re-loss and the true age. A key part of the calculations is that sulphides that are slightly super-chondritic (e.g. $^{187}Re/^{188}Os$ ratio of 0.5 in Fig. 10C) are highly sensitive to Re-loss and will readily generate unrealistically old ages or even future ages. By contrast, sulphides with highly super-chondritic ratios (e.g. $^{187}Re/^{188}Os$ ratio >10), such as those commonly found in eclogitic sulphide inclusions, are much less sensitive to Re-loss and are not included in Fig. 10C for clarity. This predictive aspect of the model can be tested, but we have not assessed the literature data in detail because we do not know whether molybdenite was lost. However, unrealistically old or future age T_{MA} are not uncommon in the literature and it is interesting to note that many of the sulphides that give spurious ages have $^{187}Re/^{188}Os$ ratios that are slightly super-chondritic (<5) or could have started with a slightly super-chondritic $^{187}Re/^{188}Os$ ratio. However, we should make it clear that both robust and spurious model ages have been found for sulphides from a wide range of $^{187}Re/^{188}Os$ ratios. Robust ages may simply reflect a lack of molybdenite loss (or formation) and spurious ages could be explained by an incorrect choice of initial $^{187}Os/^{188}Os$ ratio or a multi-stage history. Clearly, isochron ages are far the best method for dating sulphide inclusions in diamonds, but we note that differential loss of molybdenite can impact on both the age and the initial $^{187}Os/^{188}Os$ ratio derived from the isochron.

We conclude that while the formation of molybdenite and subsequent non-recovery of molybdenite during analyses might not be the only reason for disturbing Re–Os ages, the presence of molybdenite around many sulphide inclusions makes Re-loss a distinct possibility. Our clear recommendation for future work is that Raman investigation of unexposed sulphide inclusions should be an essential precursor to breaking out inclusions for analysis. Raman would show whether molybdenite was present or not, and would be the best way to assess whether molybdenite extrusion along cracks had occurred. We note that identification of molybdenite by standard electron beam-based X-ray analysis is surprisingly challenging because Mo K lines are not excited by standard operating conditions (15 kV accelerating voltage) and Mo Lα lines overlay S Kα lines are too close to resolve from by EDS. The use of higher accelerating voltages could also be problematical for thin layers

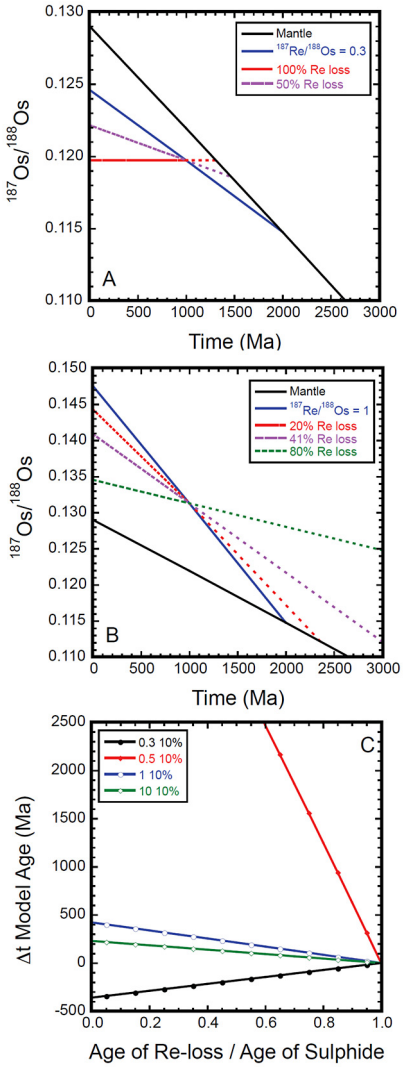

Fig. 10. A) Plot illustrating the effect of Re-loss on the Os isotopic evolution of a sub-chondritic sulphide ($^{187}Re/^{188}Os = 0.3$). In this example the sulphide was formed at 2000 Ma, but suffered Re-loss at 1000 Ma. The extreme case of 100% Re-loss will give a minimum model age of ~1300 Ma (TRD =TMA). The case of 50% Re-loss gives an older TMA of ~1500 Ma, but in all cases Re-loss will give model ages younger than the true age. B) Plot illustrating the effect of Re-loss on the Os isotopic evolution of a supra-chondritic sulphide ($^{187}Re/^{188}Os = 1$) with the same age and timing of Re-loss as above. Small amounts of Re-loss (e.g., 15%) result in a model age greater than the age of the sulphide. Increasing loss will give progressively greater ages up to the age of the Earth (in this case 41% loss). Further loss will yield ages older than the Earth and ultimately future ages (e.g. 80% loss). C) Plot of the difference in model age from the true age (Δt) as a function of the timing of the Re-loss relative to the true age of the sulphide and $^{187}Re/^{188}Os$ ratios of the sulphides, so 0.3 10% represents an initial $^{187}Re/^{188}Os$ of 0.3 and 10% Re-loss. In this case the true age of the sulphide was 2000 Ma so a Δt of 2500 Ma is essentially the age of the Earth. Again Δt scales linearly with true age.

of molybdenite because of the increased penetration depth of the electron beam. A further test of the presence of molybdenite after careful extraction of the inclusion would be to leach any remaining material from the walls of the diamond and from fractures, and to measure Re in the resulting solution.

5. Conclusions

Molybdenite was identified by Raman spectroscopy in 73 out of 80 syngenetic sulphide inclusions in Mir eclogitic diamonds. Molybdenite most commonly occurs as sub-micron-sized grains near the walls of the inclusions and is interpreted as exsolved from originally homogeneous sulphide melts (or MSS) that were encapsulated in diamond over a range of trapping temperatures. Molybdenite often accompanies chalcopyrite, and both are commonly seen inside the decompression fractures surrounding an inclusion, therefore these phases may not be quantitatively recovered during extraction of the sulphide inclusion for Re–Os dating. However, mass balance calculations indicate that molybdenite has a larger inventory of Re relative to chalcopyrite and the non-recovery of molybdenite dominates the budget of Re that is potentially lost from the analyses of the inclusion. This Re-loss may have significant effects on the resultant model ages and potentially induce significant scatter on the isochron ages of the sulphides and host diamonds.

We have modelled the potential effect of molybdenite loss on the Re–Os age systematics of diamond-hosted sulphide inclusions. For ages calculated with the isochron method, different proportions of Re loss from the inclusions would affect the quality of fit of the isochron. Re-loss could lead to unrealistically old or even future model ages being calculated, in particular if the $^{187}Re/^{188}Os$ of the sulphide is slightly super-chondritic.

The presence of molybdenite in diamond-hosted sulphide inclusions is not unique to the Mir eclogitic diamonds. Raman indicates that several other eclogitic and peridotitic diamond-hosted sulphide inclusions from Argyle, Dachine, Udachnaya, Murowa, Orapa, Letlhakane and Damtshaa also contain molybdenite. In order to militate against the problems identified in this study, we suggest that Raman investigations should precede sulphide extraction for Re–Os dating, in order to identify the presence of any molybdenite and its location within an inclusion in diamond.

Acknowledgements

This work was supported by the Natural Environment Research Council (grant number NE/M000419/1). We acknowledge The Diamond and Precious Metal Institute (Yakutsk, Russia) for providing the Yakutian diamonds. D.H. and S.K. acquired the SRXTM data at Swiss Light Source as part of proposal #20151287, and thank David Haberthur for his assistance. D.H. was funded by a DAAD PRIME fellowship during the analysis for this manuscript. We are also thankful to Peter Heard (Interface Analysis Centre, University of Bristol) for help with the FIB/SEM technique and Stuart Kearns and Ben Buse for guidance with the EPMA. The samples from Orapa, Letlhakane and Damtshaa were kindly lent by Michael Gress (Vrije Universiteit Amsterdam).

Appendix A. Supplementary material

Supplementary material related to this article can be found online at https://doi.org/10.1016/j.epsl.2018.04.037.

References

Anand, M., Taylor, L.A., Misra, K.C., Carlson, W.D., Sobolev, N.V., 2004. Nature of diamonds in Yakutian eclogites: views from eclogite tomography and mineral inclusions in diamonds. Lithos 77, 333–348. https://doi.org/10.1016/j.lithos.2004.03.026.

Anthony, J.W., Bideaux, R.A., Bladh, K.W., Nichols, M.C. (Eds.), 2003. Molybdenite — Handbook of Mineralogy. Mineralogical Society of America, Chantilly, VA. http://www.handbookofmineralogy.org/.

Aulbach, S., Stachel, T., Seitz, H-M., Brey, G.P., 2012. Chalcophile and siderophile elements in sulphide inclusions in eclogitic diamonds and metal cycling in a Paleoproterozoic subduction zone. Geochim. Cosmochim. Acta 93, 278–299.

Barnes, S.J., Cox, R.A., Zientek, M.L., 2006. Platinum-group element, gold, silver and base metal distribution in compositionally zoned sulfide droplets from the Medvezky Creek Mine, Noril'sk, Russia. Contrib. Mineral. Petrol. 152, 187–200. https://doi.org/10.1007/s00410-006-0100-9.

Barnes, S.J., Prichard, H.M., Cox, R.A., Fisher, P.C., Godel, B., 2008. The location of the chalcophile and siderophile elements in platinum-group element ore deposits (a textural, microbeam and whole rock geochemical study): implications for the formation of the deposits. Chem. Geol. 248, 295–317. https://doi.org/10.1016/j.chemgeo.2007.08.004.

Barra, F., Ruiz, J., Mathur, R., Titley, S., 2003. A Re–Os study of sulfide minerals from the Bagdad porphyry Cu–Mo deposit, Arizona, USA. Miner. Depos. 38, 585–596. https://doi.org/10.1007/s00126-002-0341-0.

Barton, P.B., 1973. Solid Solutions in the System Cu–Fe–S. Part I: the Cu–S and CuFe–S Joins. Econ. Geol. 68, 455–465. https://doi.org/10.2113/gsecongeo.68.4.455.

Brenan, J.M.B., 2002. Re–Os fractionation in magmatic sulphide melt by monosulphide solid solution. Earth Planet. Sci. Lett. 199, 257–268. https://doi.org/10.1016/S0012-821X(02)00581-2.

Bulanova, G.P., Griffin, W.L., Ryan, C.G., Shestakova, O.Y., Barnes, S.J., 1996. Trace elements in sulfide inclusions from Yakutian diamonds. Contrib. Mineral. Petrol. 124, 111–125. https://link.springer.com/article/10.1007%2Fs004100050179?LI=true.

Bulanova, G.P., Griffin, W.L., Ryan, C.G., 1998. Nucleation environment of diamonds from Yakutian kimberlites. Mineral. Mag. 62, 409–419. http://www.ingentaconnect.com/content/minsoc/mag/1998/00000062/00000003/art00013.

Bulanova, G.P., Shelkov, D., Milledge, H.J., Hauri, E.H., Smith, C.B., 1999. Nature of eclogitic diamonds from Yakutian kimberlites: evidence from isotopic composition and chemistry of inclusions. In: Gurney, J.J., Gurney, J.L., Pascoe, M.D., Richardson, S.H. (Eds.), Proceedings of the 7th International Kimberlite Conference. Red Roof Design, Cape Town, South Africa, pp. 57–65.

Bulanova, G.P., Wiggers de Vries, D.F., Pearson, D.G., Beard, A., Mikhail, S., Smelov, A.P., Davies, G.R., 2014. An eclogitic diamond from Mir pipe (Yakutia), recording two growth events from different isotopic sources. Chem. Geol. 381, 40–54. https://doi.org/10.1016/j.chemgeo.2014.05.011.

Chen, J.M., Wang, C.S., 1974. Second order Raman spectrum of MoS_2. Solid State Commun. 14, 857–860. https://doi.org/10.1016/0038-1098(74)90150-1.

Davies, R.M., O'Reilly, S.Y., Griffin, W.L., 2002. Multiple origins of alluvial diamonds from New South Wales, Australia. Econ. Geol. 97, 109–123. https://doi.org/10.2113/gsecongeo.97.1.109.

Ebel, D.S., Naldrett, A.J., 1997. Crystallization of sulfide liquids and the interpretation of ore composition. Can. J. Earth Sci. 34, 352–365. http://www.nrcresearchpress.com/doi/abs/10.1139/e17-031#.WS6ceVX1CUk.

Haggerty, S.E., 1986. Diamond genesis in a multiply-constrained model. Nature 320, 34–38. https://doi.org/10.1038/320034a0.

Harris, J.W., 1968. The recognition of diamond inclusions. Part 1. Syngenetic mineral inclusions. Ind. Diamond Rev. 28, 402–410.

Harris, J.W., 1972. Black material on mineral inclusions and in internal fracture planes in diamond. Contrib. Mineral. Petrol. 35, 22–33. https://doi.org/10.1007/BF00397374. https://link.springer.com/article/10.1007%2FBF00397374?LI=true.

Harvey, J., Warren, J.M., Shirey, S.B., 2016. Mantle sulfides and their role in Re–Os and Pb isotope geochronology. Rev. Mineral. Geochem. 81, 579–649. https://doi.org/10.2138/rmg.2016.81.10.

Lafuente, B., Downs, R.T., Yang, H., Stone, N., 2015. The power of databases: the RRUFF project. In: Armbruster, T., Danisi, R.M. (Eds.), Highlights in Mineralogical Crystallography. W. De Gruyter, Berlin, Germany, pp. 1–30.

Li, Y., Audétat, A., 2012. Partitioning of V, Mn, Co, Ni, Cu, Zn, As, Mo, Ag, Sn, Sb, W, Au, Pb, and Bi between sulfide phases and hydrous basanite melt at upper mantle conditions. Earth Planet. Sci. Lett. 355, 327–340. https://doi.org/10.1016/j.epsl.2012.08.008.

Mathur, R., Marschik, R., Ruiz, J., Munizaga, F., Leveille, R.A., Martin, W., 2002. Age of mineralization of the candelaria Fe oxide Cu–Au deposit and the origin of the Chilean Iron Belt, Based on Re–Os isotopes. Econ. Geol. 97, 59–71. https://doi.org/10.2113/gsecongeo.97.1.59.

McDonald, I., Hughes, H.S., Butler, I.B., Harris, J.W., Muir, D., 2017. Homogenisation of sulphide inclusions within diamonds: a new approach to diamond inclusion geochemistry. Geochim. Cosmochim. Acta 216, 335–357. https://doi.org/10.1016/j.gca.2017.04.039.

Mernagh, T.P., Trudu, A.G., 1993. A laser Raman microprobe study of some geologically important sulphide minerals. Chem. Geol. 103, 113–127. https://doi.org/10.1016/0009-2541(93)90295-T.

Moh, G.H., 1978. High-temperature metal sulfide chemistry. In: Tsigdinos, G.A., Moh, G.H. (Eds.), Aspects of Molybdenum and Related Chemistry. In: Topics in Current Chemistry, vol. 76. Springer-Verlag, p. 162.

O'Driscoll, B., Day, J.M., Daly, J.S., Walker, R.J., McDonough, W.F., 2009. Rhenium–osmium isotopes and platinum-group elements in the Rum Layered Suite, Scotland: implications for Cr-spinel seam formation and the composition of the Iceland mantle anomaly. Earth Planet. Sci. Lett. 286, 41–51.

Palyanov, Yu.N., Borzdov, Yu.M., Bataleva, Yu.V., Sokol, A.G., Palyanova, G.A., Kupriyanov, I.N., 2007. Reducing role of sulfides and diamond formation in the Earth's mantle. Earth Planet. Sci. Lett. 260, 242–256. https://doi.org/10.1016/j.epsl.2007.05.033.

Pearson, D.G., Shirey, S.B., Carlson, R.W., Boyd, F.R., Pokhilenko, N.P., Shimizu, N., 1995. Re–Os, Sm–Nd, and Rb–Sr isotope evidence for thick Archaean lithospheric mantle beneath the Siberian craton modified by multistage metasomatism. Geochim. Cosmochim. Acta 59, 959–977. https://doi.org/10.1016/0016-7037(95)00014-3.

Pearson, D.G., Shirey, S.B., Harris, J.W., Carlson, R.W., 1998. Sulphide inclusions in diamonds from the Koffiefontein kimberlite, S Africa: constraints on diamond ages and mantle Re–Os systematics. Earth Planet. Sci. Lett. 160, 311–326. https://doi.org/10.1016/S0012-821X(98)00092-2.

Pearson, D.G., Wittig, N., 2008. Formation of Archaean continental lithosphere and its diamonds: the root of the problem. J. Geol. Soc. 165, 895–914. https://doi.org/10.1144/0016-76492008-003.

Piña, R., Gervilla, F., Barnes, S.J., Ortega, L., Lunar, R., 2012. Distribution of platinum-group and chalcophile elements in the Aguablanca Ni–Cu sulfide deposit (SW Spain): evidence from a LA-ICP-MS study. Chem. Geol. 302, 61–75. https://doi.org/10.1016/j.chemgeo.2011.02.010.

Piña, R., Gervilla, F., Barnes, S.J., Oberthür, T., Lunar, R., 2016. Platinum-group element concentrations in pyrite from the Main Sulfide Zone of the Great Dyke of Zimbabwe. Miner. Depos. 51, 853–872. https://doi.org/10.1007/s00126-016-0642-3.

Richardson, S.H., Harris, J.W., 1997. Antiquity of peridotitic diamonds from the Siberian craton. Earth Planet. Sci. Lett. 151, 271–277. https://doi.org/10.1016/S0012-821X(97)81853-5.

Richardson, S.H., Shirey, S.B., Harris, J.W., Carlson, R.W., 2001. Archean subduction recorded by Re–Os isotopes in eclogitic sulfide inclusions in Kimberley diamonds. Earth Planet. Sci. Lett. 191, 257–266. https://doi.org/10.1016/S0012-821X(01)00419-8.

Richardson, S.H., Shirey, S.B., Harris, J.W., 2004. Episodic diamond genesis at Jwaneng, Botswana, and implications for Kaapvaal craton evolution. Lithos 77, 143–154. https://doi.org/10.1016/j.lithos.2004.04.027.

Rudnick, R.L., Eldridge, C.S., Bulanova, G.P., 1993. Diamond growth history from in situ measurement of Pb and S isotopic compositions of sulfide inclusions. Geology 21, 13–16. https://doi.org/10.1130/0091-7613(1993)021<0013:DGHFIS>2.3.CO;2. http://geology.gsapubs.org/content/21/1/13.short.

Schulze, D.J., Harte, B., Edinburgh Ion Microprobe Facility staff, Page, F.Z., Valley, J.W., Channer, D.M.D., Jaques, A.L., 2013. Anticorrelation between low $\delta^{13}C$ of eclogitic diamonds and high $\delta^{18}O$ of their coesite and garnet inclusions requires a subduction origin. Geology 41, 455–458. https://doi.org/10.1130/G33839.1. http://geology.gsapubs.org/content/41/4/455.short.

Shirey, S.B., Cartigny, P., Frost, D.J., Keshav, S., Nestola, F., Nimis, P., Pearson, D.G., Sobolev, N.V., Walter, M.J., 2013. Diamonds and the geology of mantle carbon. Rev. Mineral. Geochem. 75, 355–421. https://doi.org/10.2138/rmg.2013.75.12. http://rimg.geoscienceworld.org/content/75/1/355.short.

Sobolev, N.V., 1974. Deep-Seated Inclusions in Kimberlites and the Problem of the Composition of the Upper Mantle. American Geophysical Union, Washington D.C., p. 279.

Stachel, T., Harris, J.W., 2008. The origin of cratonic diamonds—constraints from mineral inclusions. Ore Geol. Rev. 34, 5–32. https://doi.org/10.1016/j.oregeorev.2007.05.002.

Stachel, T., Harris, J.W., 2009. Formation of diamond in the Earth's mantle. J. Phys. Condens. Matter 21, 364206. https://doi.org/10.1088/0953-8984/21/36/364206.

Stachel, T., Luth, R.W., 2015. Diamond formation—where, when and how? Lithos 220, 200–220. https://doi.org/10.1016/j.lithos.2015.01.028.

Stein, H., Scherstén, A., Hannah, J., Markey, R., 2003. Subgrain-scale decoupling of Re and ^{187}Os and assessment of laser ablation ICP-MS spot dating in molybdenite. Geochim. Cosmochim. Acta 67, 3673–3686. http://onlinelibrary.wiley.com/doi/10.1046/j.1365-3121.2001.00395.x/full.

Taylor, L.A., Milledge, H.J., Bulanova, G.P., Snyder, G.A., Keller, R.A., 1998. Metasomatic eclogitic diamond growth: evidence from multiple diamond inclusions. Int. Geol. Rev. 40, 663–676. https://doi.org/10.1080/00206819809465230.

Taylor, L.A., Liu, Y., 2009. Sulfide inclusions in diamonds: not monosulfide solid solution. Russ. Geol. Geophys. 50, 1201–1211. https://doi.org/10.1016/j.rgg.2009.11.018.

Walter, M.J., Kohn, S.C., Araujo, D., Bulanova, G.P., Smith, C.B., Gaillou, E., Wang, J., Steele, A., Shirey, S.B., 2011. Deep mantle cycling of oceanic crust: evidence from diamonds and their mineral inclusions. Science 334, 54–57. https://doi.org/10.1126/science.1209300. http://science.sciencemag.org/content/334/6052/54.

Wang, M., Guo, X., Michalak, P.P., Xia, Q., Xiao, F., Wang, W., Liu, K., 2015. Origin of the Tudun Cu–Ni sulfide deposit in the Eastern Tianshan, NW China: constraints on the geochemistry of platinum group elements. Ore Geol. Rev. 64, 445–454.

Wiggers de Vries, D.F., Pearson, D.G., Bulanova, G.P., Smelov, A.P., Pavlushin, A.D., Davies, G.R., 2013a. Re–Os dating of sulphide inclusions zonally distributed in single Yakutian diamonds: evidence for multiple episodes of Proterozoic formation and protracted timescales of diamond growth. Geochim. Cosmochim. Acta 120, 363–394. https://doi.org/10.1016/j.gca.2013.06.035.

Wiggers de Vries, D.F., Bulanova, G.P., De Corte, K., Pearson, D.G., Craven, J.A., Davies, G.R., 2013b. Micron-scale coupled carbon isotope and nitrogen abundance variations in diamonds: evidence for episodic diamond formation beneath the Siberian Craton. Geochim. Cosmochim. Acta 100, 176–199. https://doi.org/10.1016/j.gca.2012.08.034.

Zhang, Z., Lentsch, N., Hirschmann, M.M., 2015. Carbon-saturated monosulfide melting in the shallow mantle: solubility and effect on solidus. Contrib. Mineral. Petrol. 170, 1–13. https://doi.org/10.1007/s00410-015-1202-z. https://link.springer.com/article/10.1007/s00410-015-1202-z.

Zhang, Z., Hirschmann, M.M., 2016. Experimental constraints on mantle sulfide melting up to 8 GPa. Am. Mineral. 101, 181–192. https://doi.org/10.2138/am-2016-5308.

Zu, B., Xue, C., Zhao, Y., Qu, W., Li, C., Symons, D.T., Du, A., 2015. Late Cretaceous metallogeny in the Zhongdian area: constraints from Re–Os dating of molybdenite and pyrrhotite from the Hongshan Cu deposit, Yunnan, China. Ore Geol. Rev. 64, 1–12. https://doi.org/10.1016/j.oregeorev.2014.06.009.